AD-A170 854 OPTICAL DEPOLARIZATION OF THIN METAL FILMS(U) AIR FORCE 1/1
INST OF TECH WRIGHT-PATTERSON AFB OH J D HOEFT APR 86
AFIT/CI/NR-86-92T

UNCLASSIFIED F/G 14/2 NL

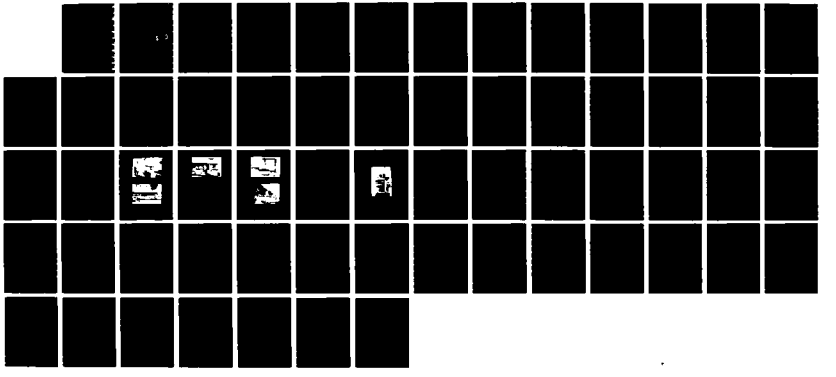

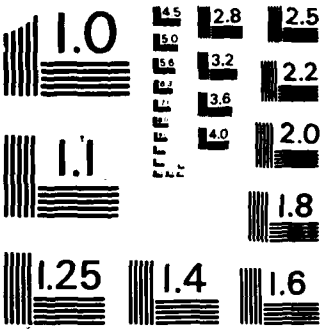

SECURITY CLASSIFICATION OF THIS PAGE (When Data Entered)

# REPORT DOCUMENTATION PAGE

READ INSTRUCTIONS BEFORE COMPLETING FORM

1. REPORT NUMBER: AFIT/CI/NR 86-92T
2. GOVT ACCESSION NO.:
3. RECIPIENT'S CATALOG NUMBER:
4. TITLE (and Subtitle): Optical Depolarization Of Thin Metal Films
5. TYPE OF REPORT & PERIOD COVERED: THESIS/DISSERTATION
6. PERFORMING ORG. REPORT NUMBER:
7. AUTHOR(s): John David Hoeft
8. CONTRACT OR GRANT NUMBER(s):
9. PERFORMING ORGANIZATION NAME AND ADDRESS: AFIT STUDENT AT: University of New Mexico
10. PROGRAM ELEMENT, PROJECT, TASK AREA & WORK UNIT NUMBERS:
11. CONTROLLING OFFICE NAME AND ADDRESS: AFIT/NR, WPAFB OH 45433-6583
12. REPORT DATE: 1986
13. NUMBER OF PAGES: 49
14. MONITORING AGENCY NAME & ADDRESS (if different from Controlling Office):
15. SECURITY CLASS. (of this report): UNCLAS
15a. DECLASSIFICATION/DOWNGRADING SCHEDULE:

16. DISTRIBUTION STATEMENT (of this Report)

APPROVED FOR PUBLIC RELEASE; DISTRIBUTION UNLIMITED

DTIC ELECTE AUG 13 1986 S D E

17. DISTRIBUTION STATEMENT (of the abstract entered in Block 20, if different from Report)

18. SUPPLEMENTARY NOTES

APPROVED FOR PUBLIC RELEASE: IAW AFR 190-1

LYNN E. WOLAVER 6 AUG 86
Dean for Research and Professional Development
AFIT/NR

19. KEY WORDS (Continue on reverse side if necessary and identify by block number)

20. ABSTRACT (Continue on reverse side if necessary and identify by block number)

ATTACHED.

AD-A170 854

DTIC FILE COPY

DD FORM 1 JAN 73 1473 EDITION OF 1 NOV 65 IS OBSOLETE

86 8 12 024

SECURITY CLASSIFICATION OF THIS PAGE (When Data Entered)

## ACKNOWLEDGMENTS

I would like to thank J.R. McNeil, G.A. Al-Jumaily, and J.J. McNally for their help in completing this masters degree. I would also like to acknowledge the rest of the Thin Films laboratory at the University of New Mexico Electrical Engineering Department for their invaluable help.

# OPTICAL DEPOLARIZATION OF THIN METAL FILMS

By

JOHN DAVID HOEFT

ABSTRACT OF THESIS

Submitted in Partial Fulfillment of the
Requirements for the Degree of

Master of Science in Electrical Engineering

The University of New Mexico
Albuquerque, New Mexico

April, 1986

# OPTICAL DEPOLARIZATION OF THIN METAL FILMS

John David Hoeft

B.S. Electrical Engineering,
New Mexico State University 1984

M.S. Electrical Engineering/Optical Engineering,
University of New Mexico 1986

All optical surfaces exhibit some degree of roughness. As a consequence of this, some of the scattered light is depolarized. Depolarization of scattered light has been previously investigated in connection with radar theory.(1) This study examined depolarization of scattered light from thin metal films using an angle-resolved optical scatterometer. The effect of varying surface morphology on the intensity of the depolarized light was investigated. The results establish that in the smooth surface limit, depolarization has little dependence on surface roughness. The intensity of depolarized light increased for surfaces which have relatively more high frequency microroughness.

TABLE OF CONTENTS

LIST OF FIGURES

# LIST OF TABLES

LIST OF PLATES

# 1. INTRODUCTION

Optical surfaces have some scatter associated with them regardless of how well they are prepared. First order vector scatter theory describes the behavior of scattered light intensity as a function of geometry and surface parameters. However, this theory does not predict optical depolarization in the plane of incidence. It is necessary to use second order vector scatter theory to predict this. The purpose of this study is to extend the scope of the research that has been done on optical depolarization of thin metal films.

## 1.1 Description of problem

The major thrust of this study was to gather data on depolarization of light intensity in the plane of incidence so that vector scatter theory could be evaluated. Measurements were made so that the results could be used for the following reasons:

To verify that our calculations based upon vector scatter theory of optical radiation are accurate,

To study how different angles of incidence influence the depolarization of optical scatter from optical surfaces,

To determine how surface morphology affects the depolarization of optical scatter from surfaces, and

To compare our results of depolarization measurements to (limited) results of other investigators, within the scope of our capability.

## 1.2 Literature review

Depolarization of waves reflected from a surface was first investigated by Barrick (1) who modeled the backscatter of radar signals using first order theory. Barrick established relationships between backscatter intensity and surface roughness in terms of the radar cross section per unit area.

Barrick's results led Church (2) to explore backscatter at optical wavelengths. Church defined the relationship between differential scatter elements and incident light intensity. He also limited his area of analysis to nonmagnetic and highly conducting surfaces. These limitations allowed him to develop a relation for intensity ratio of scattered light (Is) over incident light (Ii) that could be integrated over the front hemisphere of the surface, thus allowing the surface roughness to be calculated. In addition, this relation includes a term that represents the power spectral density. The power spectral density (PSD) function is the square magnitude of the two-dimensional Fourier transform of the surface height function. The RMS roughness is defined to be the integration of the PSD function over a

specified spatial frequency bandwidth.

Stover (3) extended Church's results to incorporate measurable quantities, such as angles of incidence ($\theta i$) and scatter ($\theta s$), aperture width ($\Omega$), scattered light intensity (Is), incident light intensity (Ii), and incident light wavelength ($\tau$). In this study, Stover's theory has been used to find the PSD and RMS surface roughness of optical thin films. These are summarized in chapter 2.

Depolarization of scattered light has been investigated theoretically by several authors. Valenzuela (4) used Rice's (5) theory to obtain depolarization from slightly rough surfaces in the plane of incidence. This was achieved using second order vector scatter theory, which takes into account multiple reflections. Second order scatter theory is beyond the scope of this study.

Depolarization in the plane of incidence was measured by Jansen (6) and Bennett (7). Jansen measured depolarization from copper thin films for a single angle of scatter. Bennett measured the retroscatter from silver and aluminum thin films. Retroscatter is the scattered light that reflects back to the incident beam from the sample.

Measurements for this study were made using Stovers method. The depolarization measurements were similar to those made by Bennett and Jansen. But in this study measurements were made in a continuous fashion across the entire front plane of incidence instead of at several discrete points.

Vector scatter theory is reviewed in Chapter 2. Chapter 3, is a description of the experimental arrangement. A description of the data collection methods is in Chapter 4. In Chapter 5, the results of the study are presented. In Chapter 6, the results are discussed. In Chapter 7, conclusions and suggested areas of future studies are made.

# 2. THEORETICAL BACKGROUND

In order to insure the calculation of the power spectral density (PSD) was being correctly performed, it was necessary to examine the development of vector scatter theory. Once this background was obtained, the performance of the scatterometer could be more fully examined.

## 2.1 Description of Power Spectral Density

The PSD of optical surfaces is derived from first order vector scatter theory. Vector scatter theory is based on the assumption that the surface RMS roughness is much smaller than the wavelength of the incident light. There are two approximate solutions to the problem of scattering from smooth surfaces. One approach is to use the Kirchoff integrals, which in principal give exact answers but several assumptions must be made to solve the integrals. The second is by making small perturbations to an ideal surface. It is this second method that will be followed here.

The relationship between scattering and surface topology has been studied in regard to radar backscatter. (8) This relationship is usually complicated, but in the smooth surface limit the connection becomes simple. Two

researchers have pioneered the application of vector diffraction theories for optical scatter, Church (9) and Elson. (10) Church's treatment will be followed in relating the scattered light to surface roughness.

Vector scattering functions have the form

$$\frac{1}{Ii}\frac{dIs}{\Omega} = \frac{C}{\tau^4} Qi(\theta i, \theta s, \phi i, \phi s, n, x_o, y_o)\, W(p,q), \qquad 2.1\ 1$$

where C is a constant, $\tau$ is the wavelength, n is the complex index of refraction, $\theta i$ and $\phi i$ are incident angles and $\theta s$ and $\phi s$ are scattered angles. Figure 2.1 depicts the angles that are used in equation 2.1 1. The scattering intensity is inversely proportional to the fourth power of wavelength ($\tau$), as in Rayleigh or Mie scattering. The quantity Qi is the optical factor, which is independent of conditions of surface and depends on the geometry of the scatter calculation. The surface factor W(p,q) is the PSD of the surface roughness. The relationship between the differential scattered light intensity and the PSD of the surface roughness is given by

$$\frac{1}{Ii}\frac{dIs}{\Omega}\,\Omega = 4\, ko^4 \cos\theta i \cos^2\theta s\, Q[r\delta]\, W(p,q)\,\Omega\,, \qquad 2.1\ 2$$

where $\Omega$ is the solid angle of the detection system, ko equals $2\pi/\tau$ is the wavenumber, and Q[r$\delta$] is the Q factor discussed in section 2.3.

Measurement of scattered light provides a method of finding the PSD. Equation 2.1 2 can be considered as the first term in the vector perturbation expansion in terms of the parameter $(k\sigma)^2$, where $\sigma$ is the RMS roughness. This theory relates the scattered light intensity as a function of angle. It does not predict depolarization in the plane of incidence. Depolarization in the plane of incidence is a second order effect, and more terms must be included for the theory to predict depolarization. By rearranging equation 2.1 2, a function for the PSD can be given by

$$W(p,q) = \frac{(Is/Ii\ (dI/\Omega))}{(4k_o^4\ \cos\theta i\ \cos^2\theta s\ Q)}. \qquad 2.1\ 3$$

Stover (3) modified this relationship to be in terms of measurable quantities, such as incident and scatter angle, incident and scatter light intensities, to be

$$W_{1/2}(\theta i,\theta s) = \frac{(Is/Ii\ 1\times10^{8}\ \tau^{3})}{(8\pi^2\cos\theta i\ \cos^2\theta s\ \Omega\ Q[f\delta])}. \qquad 2.1\ 4$$

If the wavelength is measured in microns and roughness in Angstroms, then the units of the PSD are Angstroms$^2$ per micron$^{-2}$

## 2.2 Calculation of RMS surface roughness

The RMS roughness is calculated by integrating the PSD function over a specified spatial frequency bandwidth.

The RMS surface roughness is given by

$$RMS = \left[ \int \int W(f_x, f_y)\, df_x\, df_y \right]^{1/2} . \qquad 2.2\ 1$$

## 2.3 The Q factor

The Q factor in equation 2.1 2 contains the dependence of the scattered light on the state of polarization of the incident ($\Gamma$) and scattered ($\delta$) light. The polarizations $\Gamma$ and $\delta$ are either S or P polarization. S polarization is light where the E field is orientated 90° out of the plane of incidence. P polarization is light where the E field is orientated in the plane of incidence. It also contains factors for the measurement geometry and the optical constants of the surface. The four factors are given by:

$$Q[SS] = \left[ \frac{(\epsilon-1)\cos\delta_s}{[\cos\theta_i+(\epsilon-\sin^2\theta_i)^{1/2}][\cos\theta_s+(\epsilon-\sin^2\theta_s)^{1/2}]} \right]^2 , \qquad 2.3\ 1$$

$$Q[SP] = \left[ \frac{(\epsilon-1)\sin\delta_s\ (\epsilon-\sin^2\theta_s)^{1/2}}{[\cos\theta_i+(\epsilon-\sin^2\theta_i)^{1/2}][\epsilon\cos\theta_s+(\epsilon-\sin^2\theta_s)^{1/2}]} \right]^2 , \qquad 2.3\ 2$$

$$Q[PS] = \left[ \frac{(\epsilon-1)\sin\delta_s\ (\epsilon-\sin^2\theta_i)^{1/2}}{[\epsilon\cos\theta_i+(\epsilon-\sin^2\theta_i)^{1/2}][\cos\theta_s+(\epsilon-\sin^2\theta_s)^{1/2}]} \right]^2 , \qquad 2.3\ 3$$

$$Q[PP] = \left[ \frac{(\epsilon-1)(\epsilon-\sin^2\theta_i)^{1/2}(\epsilon-\sin^2\theta_s)^{1/2}\cos\delta_s - \epsilon\sin\theta_i\sin\theta_s}{[\epsilon\cos\theta_i+(\epsilon-\sin^2\theta_i)^{1/2}][\cos\theta_s+(\epsilon-\sin^2\theta_s)^{1/2}]} \right]^2 . \qquad 2.3\ 4$$

Where the first subscript is the incident light

polarization and the second is the collected scattered light polarization. Using these expressions, in the plane of incidence where $\Phi s = 0°$, the Q factor equals zero for cross polarized measurements. In the limit of small scattering angles $\theta s = \theta i$, the Q factor reduces to the reflectance (R[S]) of the surface.

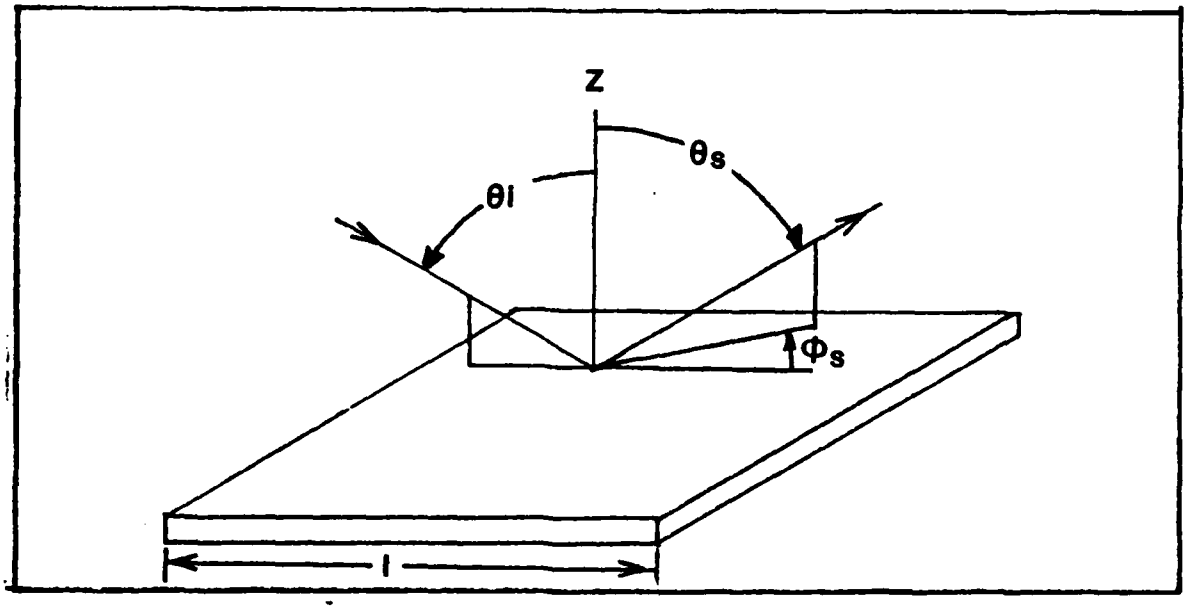


Figure 2.1 Definition of all angles pertinent to the calculation.

# I. EXPERIMENTAL ARRANGEMENT

Over the last few years, the angle-resolved optical scatterometer at the University of New Mexico Thin Films Laboratory has been continuously upgraded to incorporate new areas of research. The original system consisted of an HeNe laser as a light source, an optical system consisting of spatial filters and lenses to remove higher diffraction orders and focus the beam, and a detection system consisting of a photo multiplier tube (PMT) and a rotating table. The entire system was enclosed in a darkened part of a clean room so that background light would not affect measurements. This system could measure optical scatter in both transmissive and reflective optical components. It could measure scattered radiation from optical components at near normal incidence, and throughout one half of the plane of incidence.

For this study, it was necessary to make several upgrades. The scatterometer, after the improvements, is shown in plate I.1. These improvements and the increased capabilities are listed below:

Implementing a position encoder to allow more accuracy in measuring the angular position of the detector;

Installing an argon ion laser to permit multi-wavelength scatter measurements;

Implementing new computer programs for improved data collection and increased flexibility in analysis of the raw data;

Implementing polarization measurement capabilities;

Installing a new analog-to-digital converter (ADC) to provide more precise measurements of the scattered light intensities.

## 3.1 Lasers

Two lasers, an argon ion and an helium neon, provide light for the optical system, see plate 3.2. The HeNe laser is a 15 mw continuous wave (CW) laser operating at 633 nm. The argon ion laser is a variable power CW laser with a maximum power of 7 w, capable of operating at 350, 488 and 514 nm. Both of the lasers are polarized in the S direction. This flexibility in power and wavelength allows the measurement of dielectric films at half and full wave optical thicknesses, and permits the measurement of optical components with lower reflectance.

## 3.2 Optical system

The optical system consists of a spatial filter, apertures, and lenses. The output from the lasers passes through the optical system and is focused onto the detector. The system configuration is shown in plate 3.2, 3.3, and in figure 3.1. In this improved system, the polarized beam emitted from the laser passes through a

half wave plate which rotates the beam polarization to the desired direction. The beam is passed through a polarizer to reject the undesired polarization. This beam is turned by two beam steering mirrors; these align the beam across the center of the detection system. The aligned beam passes through another polarizer to increase the rejection ratio. The beam is chopped so that a heterodyne detection system can be used to measure the light intensity. The beam can pass through a set of neutral density filters that reduce the beam intensity and thus allow the specular beam to be measured. The beam is then passed through a spatial filter which removes all spatial frequencies except for the central order. The beam is focused on the detector collecting lens using a high-quality, low-scatter focusing lens. This is done so the measurements are made in the far field. To terminate any stray light from the focusing lens, the focused beam is passed through several apertures. Another polarizer is placed in front of the detector. The direction of this polarizer can be orientated to measure light of the same polarization as the input or to measure the cross polarized signal. This arrangement including multiple polarizers yields a polarization rejection ratio of 10000:1. When polarization measurements are not being made, the polarizers and the half wave plate are removed from the system.

## 3.3 Detection system

The detection system shown in plate 3.4 is used for measuring the intensity of scattered light as a function of angle. Although it can measure optical scatter either in transmission or reflection, in this work the instrument was only used in reflectance. The detection system consists of a rotatable table on top of a stable surface. A fiber optic and PMT are mounted on the table and can be rotated over 270°. A sample mount with five degrees of freedom is used to hold coating samples. The table position is monitored by the computer through an optical position encoder. The resolution of the encoder is .015 ± .007 degrees per count, which allows for a precise measurement of table position relative to the specular beam. All of the measurements are made in the same direction to reduce position errors. The intensity of the scattered light is monitored by the computer through a lock-in amplifier and an ADC.

The light reflected from the sample passes through the final polarizer and is collected by the lens and is passed to the detector. See plate 3.5. This arrangement has a collecting lens, a field stop and a fiber optic. Figure 3.2 illustrates the geometry of the fiber optic collection system. The lens focal length is 16 mm

and the lens diameter is 4 mm. The image of the fiber optic is larger than the image of the field stop. The lens of figure 3.2 is the aperture stop of the system: the detector solid angle ($\Omega$) is limited by the aperture stop to .00011 steradians (sr). From figure 3.2, it can be seen that all rays originating from a circle of diameter $\emptyset$ enter the fiber and are detected. Using the dimensions of figure 3.2, $\emptyset$ = 7.5 mm. The illuminated spot on the sample is 2.0 mm diameter and is within this 7.5 mm diameter area. The field of view of the system is limited by the field stop to a collection area of 17.6 mm diameter on the sample. This arrangement also reduces the influence of vibrations in the measurements.

By assuming that the light is approximately a plane wave at the optic a minimum sampling interval can be found. A minimum sampling interval is found by considering the angle subtended by the detector collecting lens (aperture stop). This angle is the amount that the detector would have to be moved if the detector were not to measure the same scattered light more than once. From the dimensions in figure 3.2 this angle is .68°. Because the measurements are made with smaller sampling intervals than .68° the data is averaged in a manner that warrants discussion. The angle subtended by the detector relates to a bandwidth of spatial frequencies for each data

point. Therefore each data point on a PSD curve corresponds to averaging the scattered light over a bandwidth of spatial frequencies, which will be called Spatial Frequency Width (SFW). This width is dependent on the scatter angle and is given by

$$SFW = Fmax - Fmin \qquad 3.7\ 1$$

$$SFW = \frac{\sin(\theta s+.34°)-\sin(\theta i)}{\tau} - \frac{\sin(\theta s-.34°)-\sin(\theta i)}{\tau}. \qquad 3.3\ 2$$

The maximum value of the SFW occurs for a frequency of 0. microns$^{-1}$ which corresponds to $\theta s = 0°$ and is 0.0187 microns$^{-1}$. In measurements of RMS roughness, the largest angle used is 70°, this corresponds to a spatial frequency of 1.485 microns$^{-1}$, and a SFW of .0064 microns$^{-1}$. To decrease the SFW of each measurement point it is necessary to reduce the size of the detector collecting lens.

One method of determining the sensitivity of the system is to determine the minimum detectable BRDF of the system. This is set by the the dark current of the system, and is $6.6 \times 10^{-8}$ sr$^{-1}$. The maximum BRDF scatter is the inverse of the solid angle of detection ($\Omega$) and is 9091. sr$^{-1}$. To measure a sample with the maximum sensitivity (which corresponds to the minimum BRDF), it is necessary to reduce the sampling rate by an order of magnitude of what is normally used. This is necessary in

order to accommodate increase in the time constant of the measurement apparatus. Including this, the dynamic range of the system is eleven orders of magnitude ($1.37 \times 10^{11}$). Another method to characterize the sensitivity of the scatterometer system is to consider the equivalent system RMS roughness. This is found by measuring the scatter from the incident laser beam and analyzing this to find the equivalent system RMS roughness. The equivalent system RMS roughness is measured every time the scatterometer is used and is typically less than 3.0 Angstroms, as measured within the spatial frequency bandwidth of the system (.014 microns$^{-1}$ to 1.6 microns$^{-1}$).

The light that reaches the end of the fiber optic is dispersed by a piece of ground glass to ensure that a direct beam of light does not reach the PMT. See figure 3.3. The beam passes through an interference filter centered at the wavelength of interest to minimize any problems caused by stray light. A resistor converts the PMT current into a voltage, and this is measured by a lock-in amplifier. This amplifier has ranges from 100 mV to 1 μV full scale, which corresponds to 10 μA to 100 pA. Because the dark current of the PMT is approximately 2 pA in the 1 Hz bandwidth of the lock-in, the 1 μV range is not normally used.

The lock-in amplifier output, zero to ten volts, is applied to the ADC of the computer. All the position and intensity measurements are recorded directly by the computer. This technique not only reduces the difficulty of making measurements, but it also provides better records and removes some of the art of making measurements.

## 3.4 Computer interfaces

The computer used to make these measurements is a Digital LSI-11/03; see plate 3.6. Although another computer, the LSI-11/23, was used for software development, the software runs on either machine. The computer uses a menu-driven control program listed in Appendix 1 that provides more flexibility in measurement techniques. The sensors on the detection system give the computer information about the position of the detector and the intensity of the light signal. The computer continuously monitors the position of the detector and the intensity of the light.

Plate 3.1 The scatterometer system.

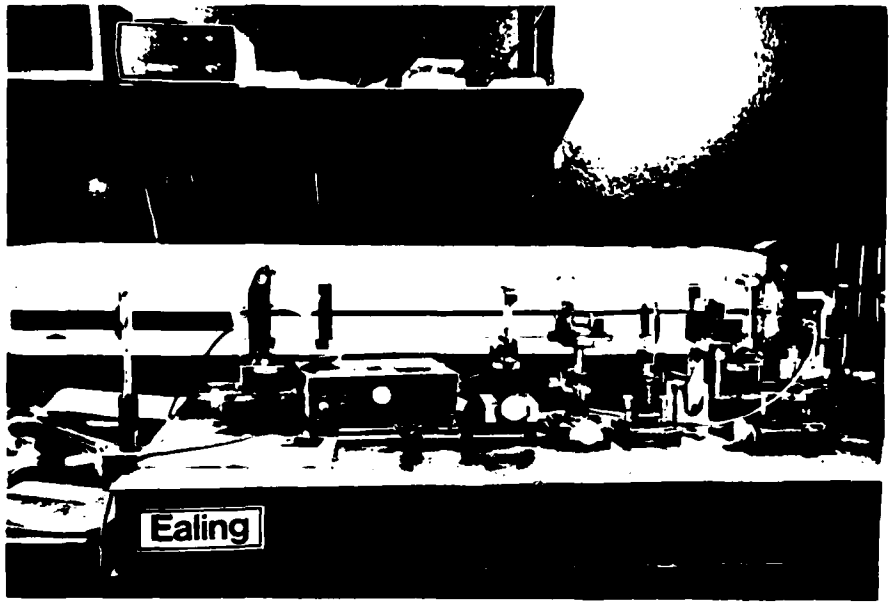


Plate 3.2 Argon and HeNe laser at start of optical system.

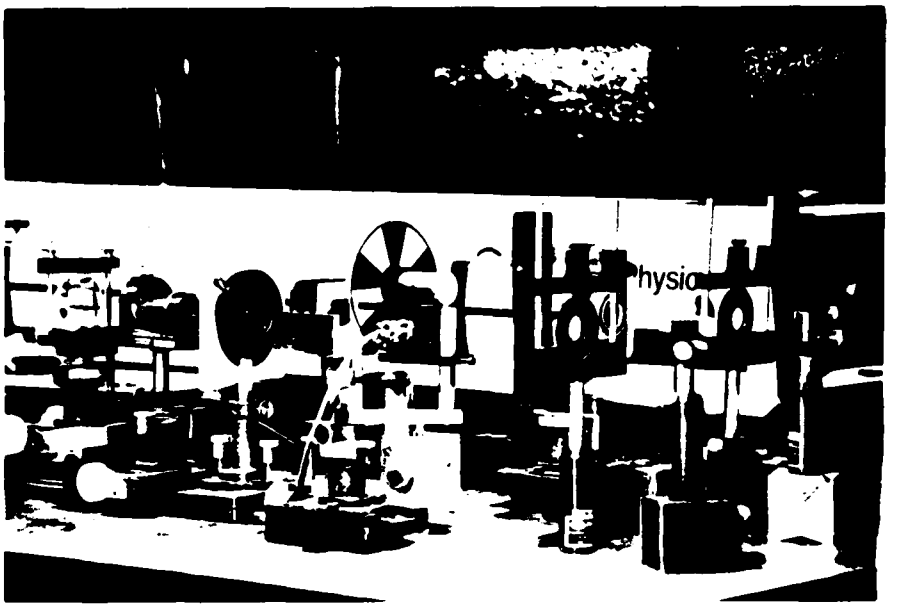

Plate 3.3 Optical system from lasers to scatterometer.

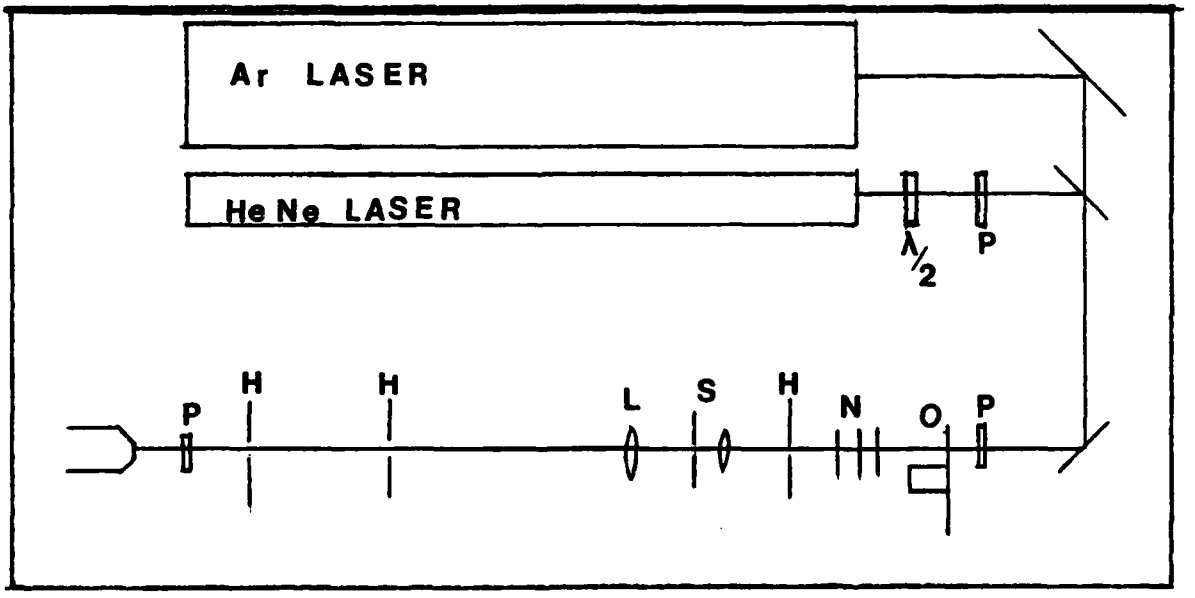


Figure 3.1 The optical system from lasers to fiber optic light collector. P-polarizers, O-optical chopper, N-neutral density filters, H-scatter limiting aperture, S-spatial filter, L-focusing lens.

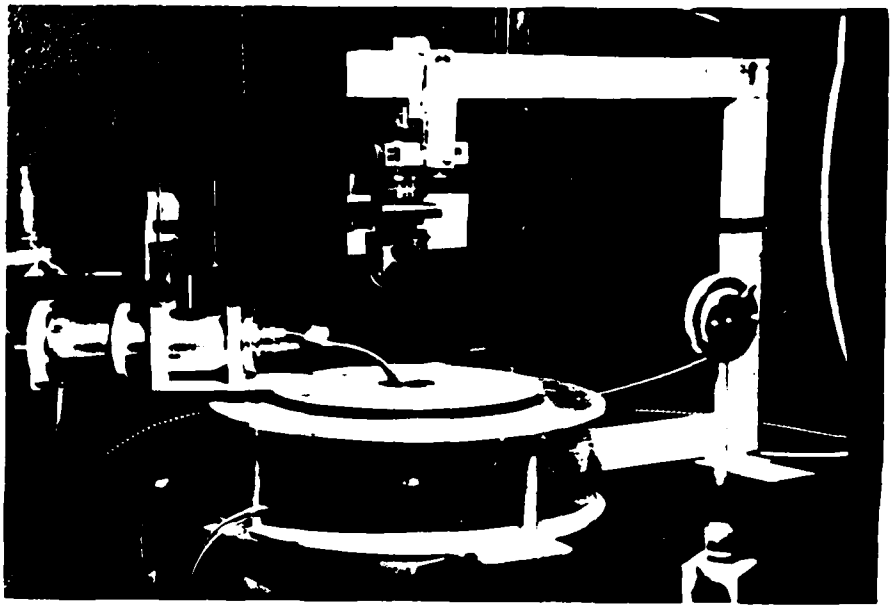

Plate 3.4 Detection system.

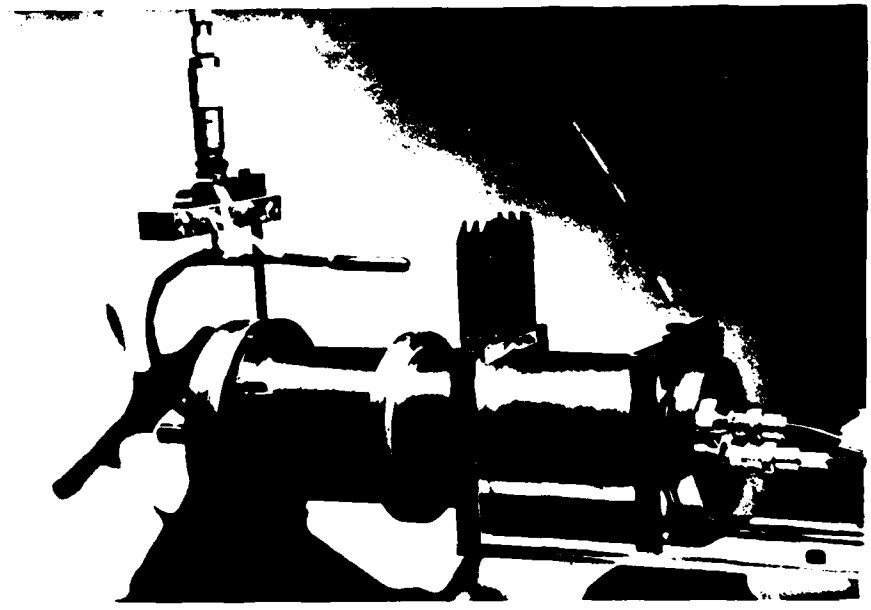

Plate 3.5 Fiber Optic light collector and the photo multiplier tube.

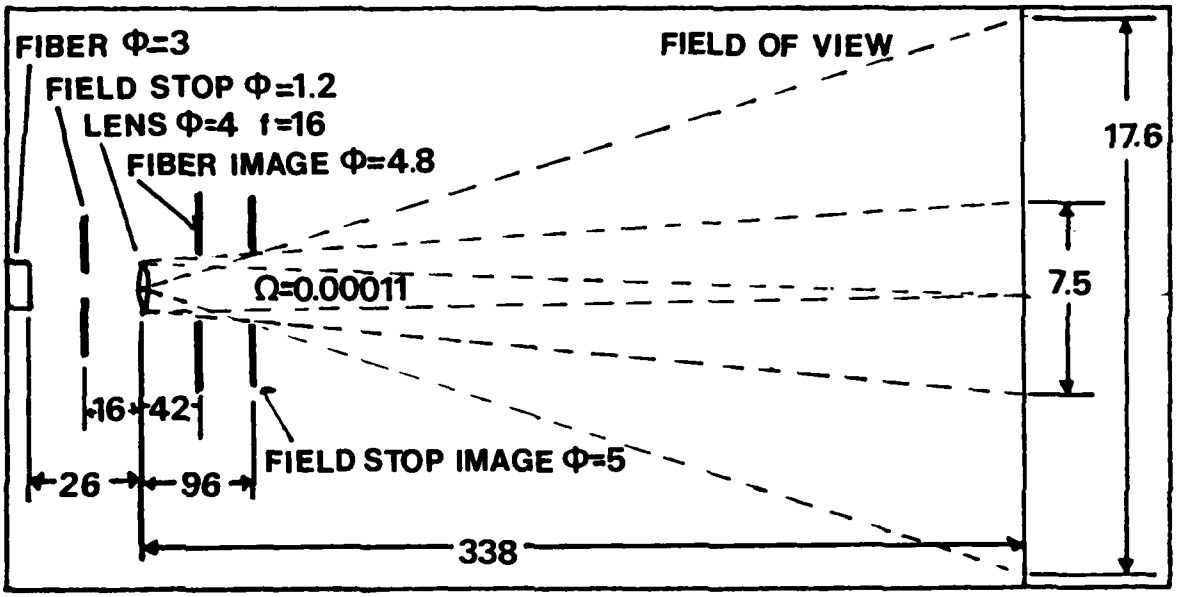


Figure 3.2 Dimensions of the detector where Ø is the diameter and all measurements are made in millimeters.

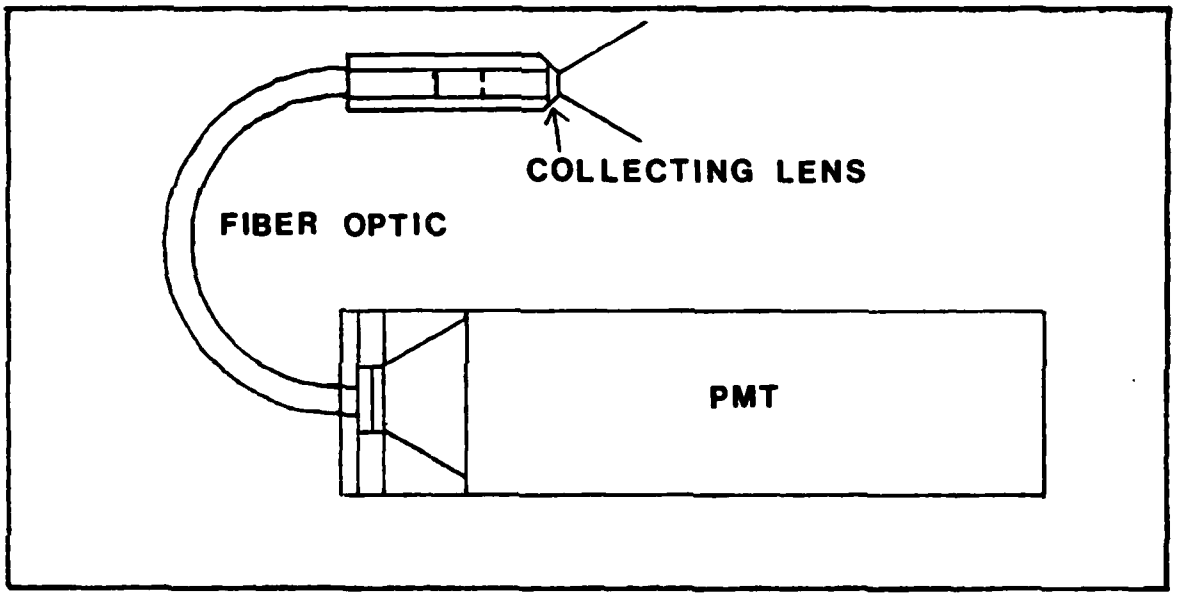


Figure 3.3 The fiber optic light detector.

Plate 3.6 The LSI-11-03 computer.

# 4. DATA COLLECTION

In this work the data was collected and analyzed using a computer. The program used for data collection was called SCAT.FOR and was a menu driven control program which provided the following options:

Initializing the scatterometer control program;
Measuring system background noise;
Measuring sample scatter;
Calculating and displaying PSD curves;
Calculating and displaying BRDF curves;
Printing and plotting raw data;
Testing computer ports.

These options could be requested in any order after the scatterometer control program was initialized, and the system background noise was measured.

## 4.1 Verification of the PSD and RMS calculations

In order to verify the PSD and RMS roughness calculations, the following procedure was used. A formula to simulate constant scatter intensity which can be used to calculate the RMS roughness is given by:

$$RMS = \int \int PSD \, d\theta s \, d\bar{\theta}s \qquad 4.1\ 1$$

$$= \frac{[\ (Is/Ii)\ \tau^4\ (1\times10^9)\ 2\pi\ \tan\theta s\ ]^{1/2}}{[.00011\ (16\pi^2)\ \cos\theta i\ ]^{1/2}} \quad . \qquad 4.1\ 2$$

A constant voltage signal was applied to the lock-in amplifier to simulate a constant scatter intensity for all angles. The computer then calculated the PSD and RMS

roughness. The results are presented in Chapter 5. These values were then compared to the mathematically calculated value for the RMS roughness.

## 4.2 Data collection procedure

The following procedure was used to measure the optical scatter data and analyze the results. First, the scatterometer operating conditions were initialized by inputting the number of averages to make for each data point, inputting the range of the scan, inputting the wavelength, setting the sampling interval, and identifying the graphics output device. Second, the system background noise was measured and subsequently accounted for in the calculations.

To measure the scatter, the reflected specular beam must be found. This was accomplished by scanning the detector across the reflected specular beam and recording data every 0.015°. This data provides a profile of the specular beam. To obtain a more accurate value for the intensity of the specular beam, the beam intensity profile data was averaged over the center 0.4°. Then a scatter measurement was made from the center of the specular beam to the specified range. The data at each sampling point consisted of scattered intensity (Is); and scatter angle

·9z·. Two sampling intervals were used in data collection. From the center of the specular beam to 0.6° from the center, data was collected every 0.015°; from 0.6° to 90° a sample interval of 0.2° was used. The system background noise was measured, and a PSD and RMS roughness were calculated for the system noise.

A maximum acceptable value for the system background noise was set at 3.0 Angstroms. The system equivalent roughness was never significantly less than 3.0 Angstroms, and this value therefore represented a reasonable standard. If the equivalent system roughness was greater than 3.0 Angstroms, the system was realigned.

Once the system was properly aligned, the sample was placed in the sample holder and adjusted so the detector was in the plane of incidence. The sample was rotated to the desired angle of incidence. A measurement of the scattered light was made in a manner similar to that used for the background system noise measurement.

When scattered light was measured for non-normal incident light, the range of the scan was adjusted so data was not collected for angles greater than 90° from the normal to the sample. This was done automatically by the computer.

## 4.3 Procedure for depolarization measurement

The scattered light was first measured for the same polarization as that of the incident light ( i.e. SS or PP polarization). Where the first polarization is the input light polarization and the second is the collected light polarization. Then the scattered light was measured with crossed polarizers (i.e. SP or PS). Depolarization is defined as the ratio of these two sets of data, SP/SS or PS/PP. The depolarized light was measured across the entire front plane of incidence of the surface.

## 4.4 Data analysis

The PSD curves were displayed by the computer. In this part of the program the PSD was calculated from the measured scattered light data, and the RMS roughness was calculated from the PSD. The spatial frequencies over which measurements were made were also calculated. The equations used to make these calculations are:

$$PSD(i) = \frac{\tau^4 \quad Is}{(\Omega \; Ii \; 16\pi^2 \; \cos\theta i \; \cos^2\theta s \; Q)}, \qquad 4.4\text{-}1$$

$$= \frac{Is \quad \tau^4 \quad 1\times10^6}{[Ii \; (.00011) \; (16\pi^2) \; \cos\theta i \; \cos^2\theta s \; Q]} \; . \qquad 4.4\text{-}2$$

Here $\Omega$ is the solid angle of the detector in steradians,

$$Freq(i) = \frac{(\sin\theta s - \sin\theta i)}{\tau}, \qquad 4.4\text{-}3$$

eg. RMS(i) =

[freq(i+1)-freq(i)][PSD(i)freq(i)+PSD(i+1)freq(i+1)]2π 2.
4.4 4

Note the values were calculated point by point, starting at the edge of the specular beam, and the units are Angstroms$^2$ per microns$^{-2}$.

Because RMS is an integrated quantity, RMS(i) is the differential roughness from the edge of the specular beam to the angle θs. The edge of the specular beam is defined as the point at which the scattered light intensity is twice the system background noise, this is usually .5°. After calculating these quantities, the computer plots the PSD versus spatial frequency curves and prints out the RMS roughness. Also printed are values for spatial frequency bandwidth of the measurement, the total integrated scatter calculated from the RMS roughness in ppm, and the amount of scattered light divided by the amount of specular light in ppm. This gives accurate numbers for the absolute RMS surface roughness in a specific spatial frequency bandwidth.

In the fifth part of the program the bidirectional reflectance distribution function (BRDF) of the data was calculated and plotted versus scatter angle. The equation for BRDF was given by Harvey (11) as

$$BRDF = \frac{Is}{[Ii\ \Omega\ \cos(\theta s)]}. \qquad 4.4\ 5$$

Note that BRDF has units of inverse steradians ($sr^{-1}$).

There was a second program that was used to analyze depolarization and scatter data called SCTPLO.FOR. See Appendix 2. This program plots SS, SP, PS, PP, SP/SS, or PS/PP versus angle or versus direction cosine. The plots in chapter 5 were made with this program.

# 5. RESULTS

Measurement of depolarization in scattered light intensity was performed using an angle-resolved optical scatterometer. Data is presented here as a result of examining the effects of angle of incidence, angle of scatter, film material and surface morphology on intensity of the depolarized light.

## 5.1 Verification of PSD and RMS calculations

To verify that the calculation of the PSD and RMS was correct, the procedure described in Chapter 4 was used. The results are tabulated in table 5.1. Four test samples were used with different ratios of Is/Ii. This was done to insure that the model was correct over the complete range of sample roughness encountered. The calculated RMS values were obtained by direct substitution in equation 4.1 2. The correlation between the calculated and measured values illustrates that the analysis program is calculating the correct value for the PSD and RMS roughness. For these calculations, normal incidence was used. For normal incidence the Q[SS] factor is equivalent to the reflectance (R[S]) which was set equal to 1.0 for this test.

A series of tests were also performed to examine the significance of using the approximated value for Q[SS] (Q[SS]≈R[S]) instead of the exact expression in equation 2.3 1. A ratio for the correct RMSQ (RMS roughness including Q[SS]) roughness to the approximation RMS (RMS roughness with Q[SS] = R[S]) roughness was calculated as a function of reflectance for various angles of incidence, and the same shape of PSD curve. Figure 5.4 illustrates the PSD curves that were used to find the correction factor curve. This plot illustrates the PSD as a function of spatial frequency. The values for the correction factor were found by using different indexes of refraction in the calculation for the sample PSD curves, and then averaging the four RMS roughness results. The results are plotted in figure 5.1. Figure 5.1 illustrates that for samples with a relatively high reflectance (0.9 ≤ R), the correction factor is approximately 1.0. Figure 5.1 also illustrates that the correction factor decreases with increasing angle of incidence, which indicates that the Q factor affects the magnitude of the RMS roughness. Figure 5.2 illustrates that the Q factor also affects the shape of the PSD curve. Figure 5.2 is a plot of the Q factor versus scatter angle for an incident angle of 2° and for various materials. This plot illustrates that the Q factor deemphasizes the high spatial frequency microroughness and emphasizes the low spatial frequency

microroughness, especially for low reflectance films. Figure 5.3 is a plot of the Q factor versus scatter angle for an incident angle of 30° and for various materials. Note that for other PSD curve shapes, the correction factor curve would be slightly different because the correction factor is the integration of the PSD curve including the Q factor.

Very little experimental data involving depolarization of optical scattered light is presently available in the literature. Among the data which was available is that of Bennett (7). Of primary interest in Bennett's investigation was the amount of retroscatter, because first order vector scatter theory and experimental data had the greatest discrepancy for retroscatter. To match the conditions that were used by Bennett as close as possible, a glass substrate was coated with silver, and the retroscatter light intensity was measured. Table 5.2 lists the values for retroscatter ratios for results from our measurements (UNM) and those of Bennett (NWC).

## 5.2 PSD results for various samples

Figure 5.4 illustrates the PSD versus spatial frequency curves for a number of the copper samples studied. Four samples with roughness ranging from 18 to

95 Angstroms RMS roughness in the spatial frequency bandwidth from .014 to 1.485 microns$^{-1}$ are plotted.

Figure 5.5 illustrates two PSD curves for two molybdenum samples. These samples had roughness of 45 and 77 Angstroms RMS roughness. These samples were used in comparisons with copper samples. The molybdenum is dominated by low spatial frequency microroughness compared to the distribution of microroughness of the copper samples.

## 5.3 Depolarization as a function of surface morphology

Figure 5.6 displays the depolarization for various copper samples with various RMS roughness and $\theta i = 60°$. The vertical scale is the ratio of the BRDF of the crossed polarized light to the BRDF of the light that was in the same direction as the incident light. The horizontal axis is direction cosines which were presented by Harvey (11) and are $\cos(\theta s) - \cos(\theta i)$. By plotting the data using this method it is centered and symmetric on the plot making it easier to compare. For some of the plots, the horizontal extent of the plot is limited because the amount of scatter for that angle was comparable to the noise level of the system. Figure 5.6 illustrates the

variation of depolarized light intensity as a function of RMS roughness. Figure 5.7 illustrates depolarization from a sample of copper and a sample of molybdenum with $\theta i$ = 60°. This depicts the large difference in scatter characteristics of samples having different surface morphologies. The molybdenum has much lower depolarization than the copper. Figure 5.8 illustrates the depolarization for the samples for P input polarized light, and an angle of incidence of 60°. This indicates that the amount of depolarization changes for the molybdenum while it is approximately constant for copper.

## 5.4 Depolarization as a function of angle of incidence

Figure 5.9 illustrates the variation of depolarization versus direction cosines at several different angles of incidence, for the copper sample with 60 Angstroms of RMS roughness. Depolarization is plotted for $\theta i$ = 4°, 30°, 60° and 82°. Figure 5.10 illustrates the same sample but with P input polarization and $\theta i$ = 30°, and 60°. Figure 5.11 illustrates depolarization versus direction cosines from the molybdenum sample with 45 Angstroms of RMS roughness, with $\theta i$ = 30° and 60°. Figure 5.12 illustrates the depolarization as a function

of angle for the same molybdenum sample with P input polarization. This indicates that for this molybdenum sample, the amount of depolarization depends on angle of incidence.

Table 5.1

Verification of correct calculation of PSD and RMS with constant scatter data.

| Is/Ii | Calculated RMS | Measured RMS |
|---|---|---|
| $1.\times10^{-4}$ | 118.04 | 118.71 |
| $1.\times10^{-3}$ | 38.35 | 38.62 |
| $1.\times10^{-2}$ | 11.88 | 11.90 |
| $1.\times10^{-1}$ | 3.73 | 3.76 |

TABLE 5.2

Comparison of UNM retroscattering results to those of Bennett (7) at the Navel Weapons Center (NWC) for 60° angle of incidence on silver samples.

| | UNM | NWC | Theoretical |
|---|---|---|---|
| PP/SS | 11.9 | 8.2 | 40 |
| SP/SS | .114 | .215 | 0 * |

* Note that the theoretical value for first order vector scatter theory dose not predict any depolarization in the plane of incidence.

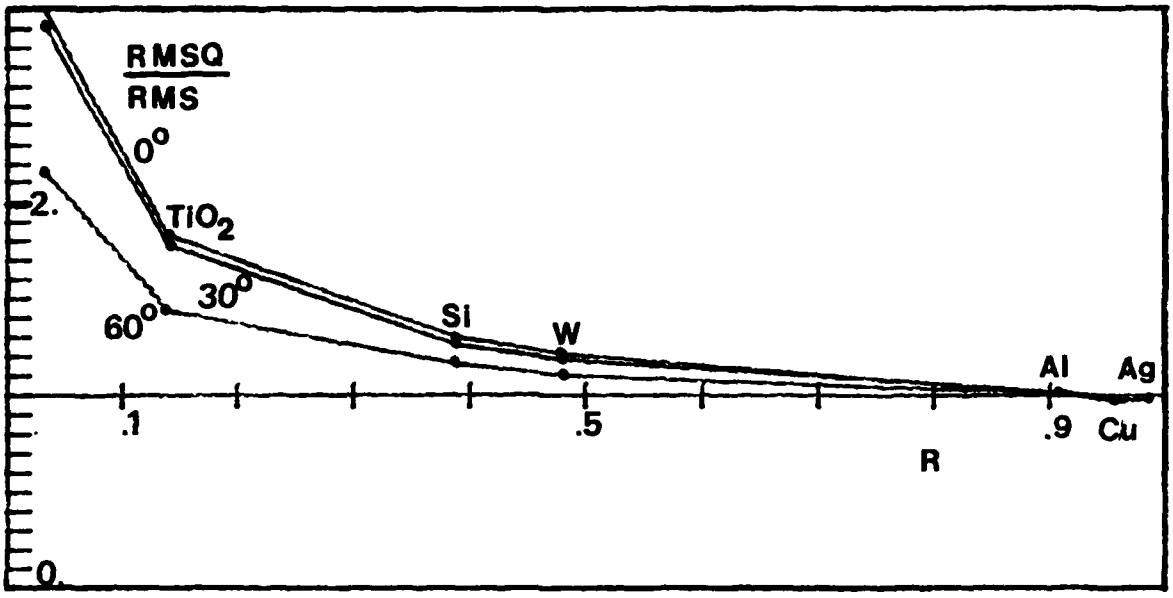


Figure 5.1 The correction factor (RMSQ/RMS) versus the reflectance of the thin film material for near 0°, 30°, and 60° angle of incidence for the particular PSD characteristic illustrated in figure 5.4. Note each point correspond to a different material.

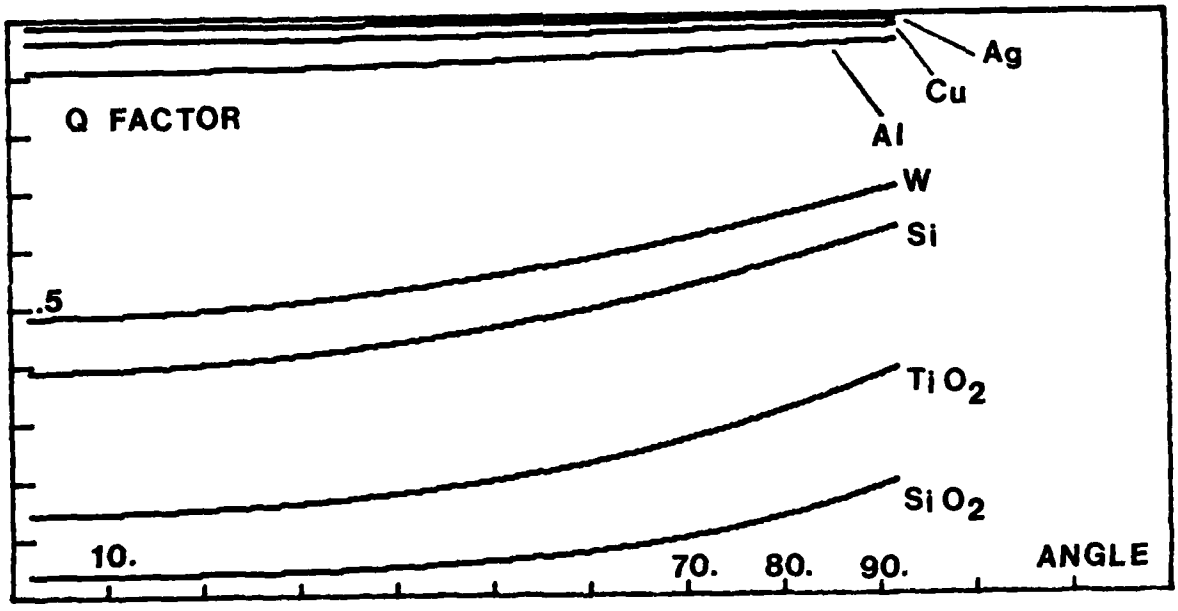


Figure 5.2 Q factor versus scatter angle (θs) for an incident angel of 2° and various materials.

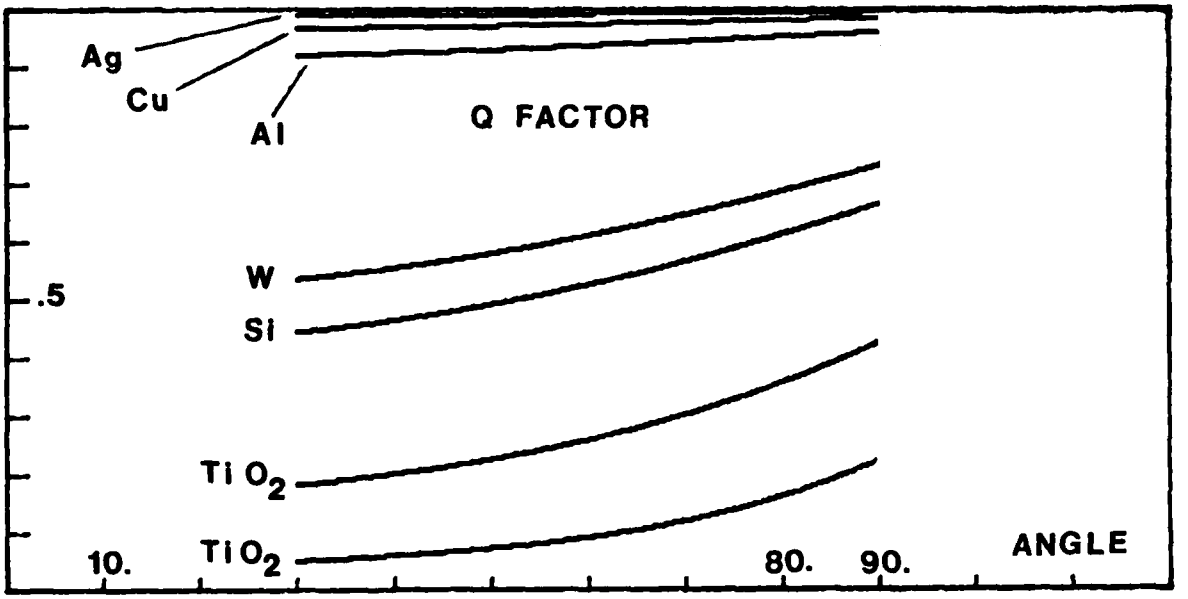


Figure 5.3 Q factor versus scatter angle (θs) for an incident angle of 30° and various materials.

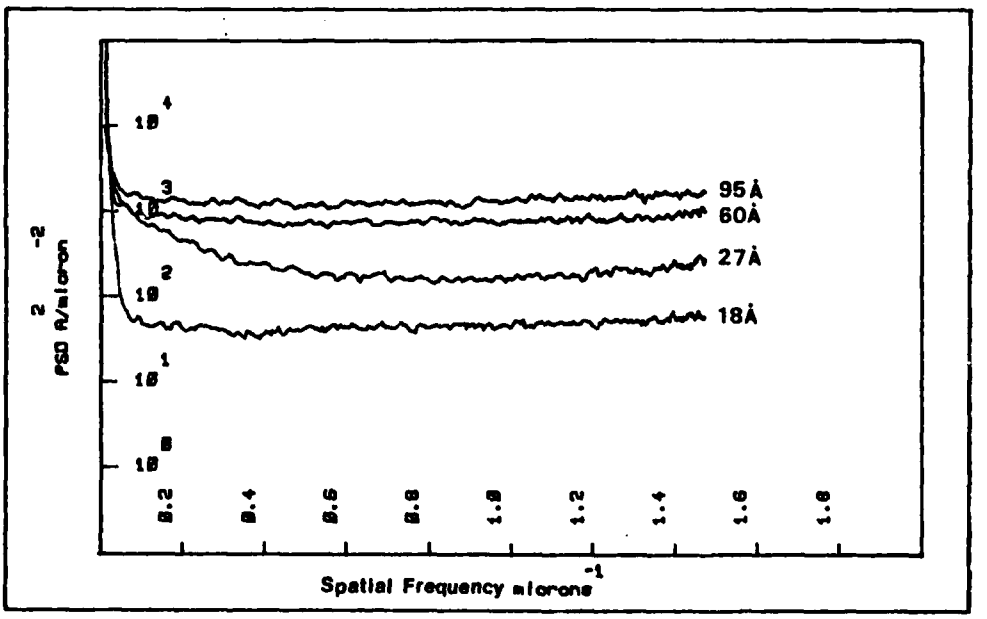


Figure 5.4 PSD versus Spatial frequency for copper samples with roughness ranging from 18 to 95 Angstroms RMS roughness, and near normal angle of incidence.

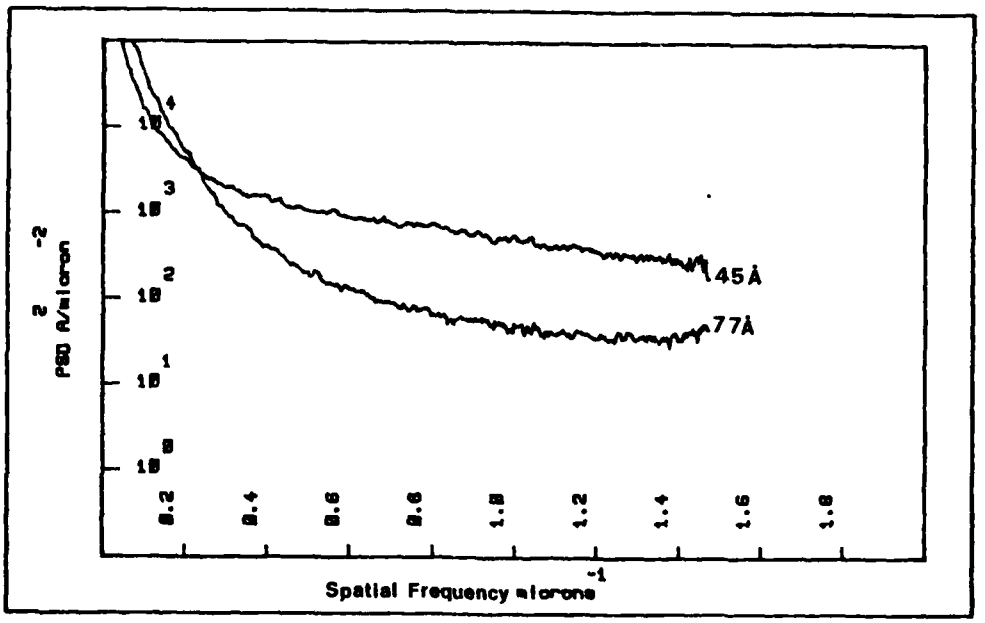


Figure 5.5 PSD versus spatial frequency for molybdenum samples with 45 and 77 Angstroms of RMS roughness, and near normal angle of incidence.

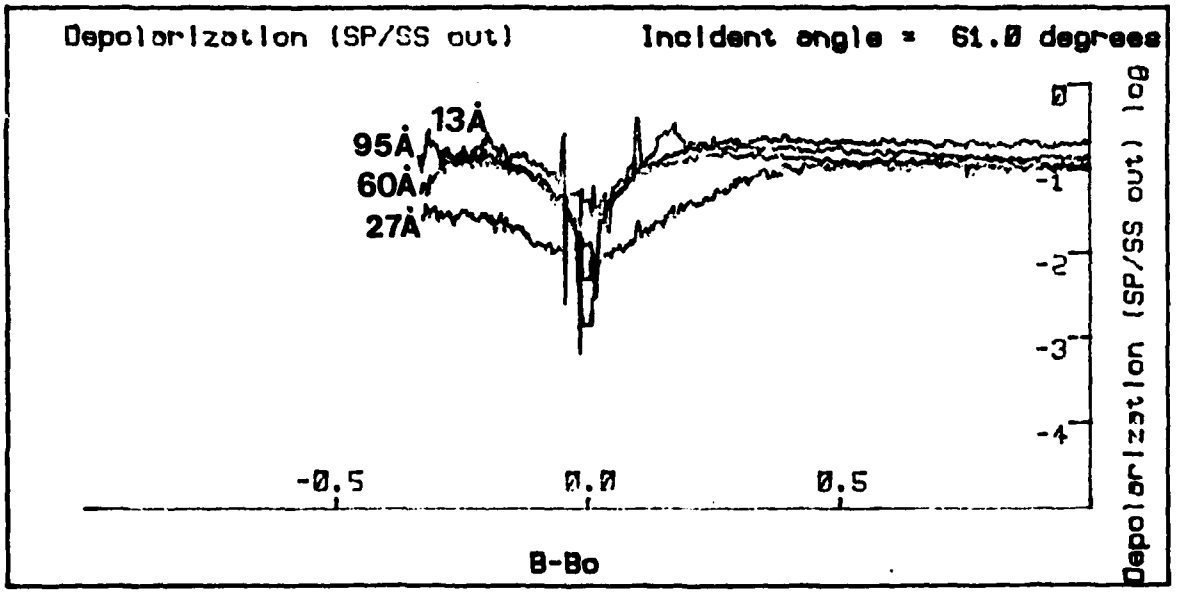


Figure 5.6 Depolarization versus direction cosines for copper samples with RMS roughness of 18, 27, 60, 95 Angstroms and θi = 60°.

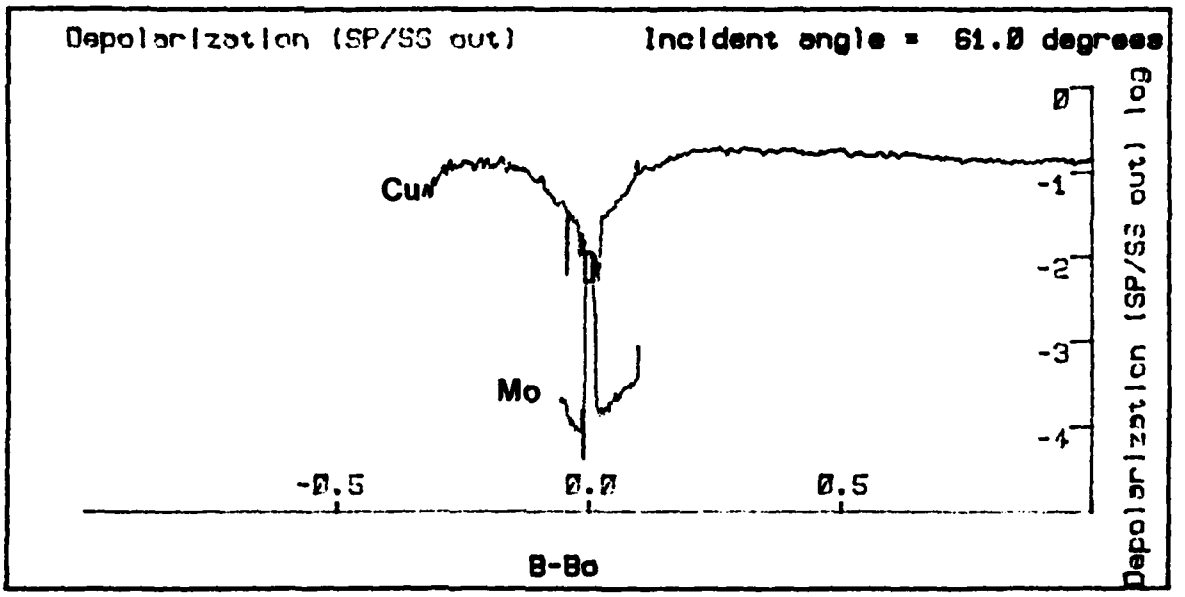


Figure 5.7 Depolarization versus direction cosines for the copper sample with RMS roughness of 60 Angstroms and for the molybdenum sample with roughness of 77 Angstroms, and $\theta i = 60°$.

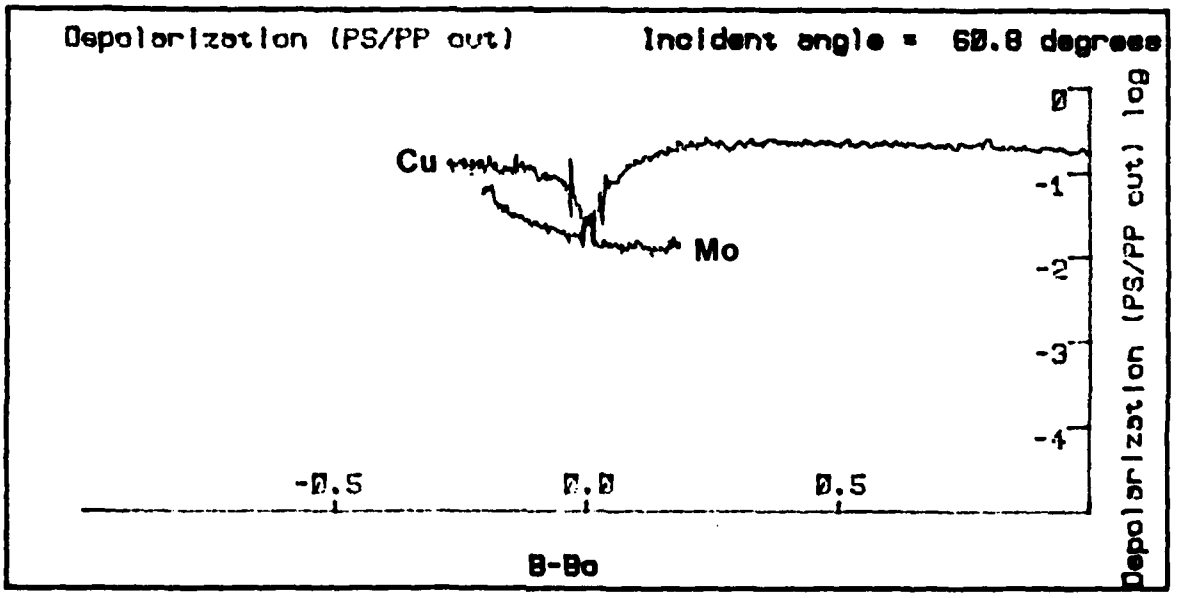


Figure 5.8 Depolarization versus direction cosines for the copper sample with roughness of 60 Angstroms and for the molybdenum sample with 77 Angstroms of roughness and $\theta i = 60°$, with P input polarization.

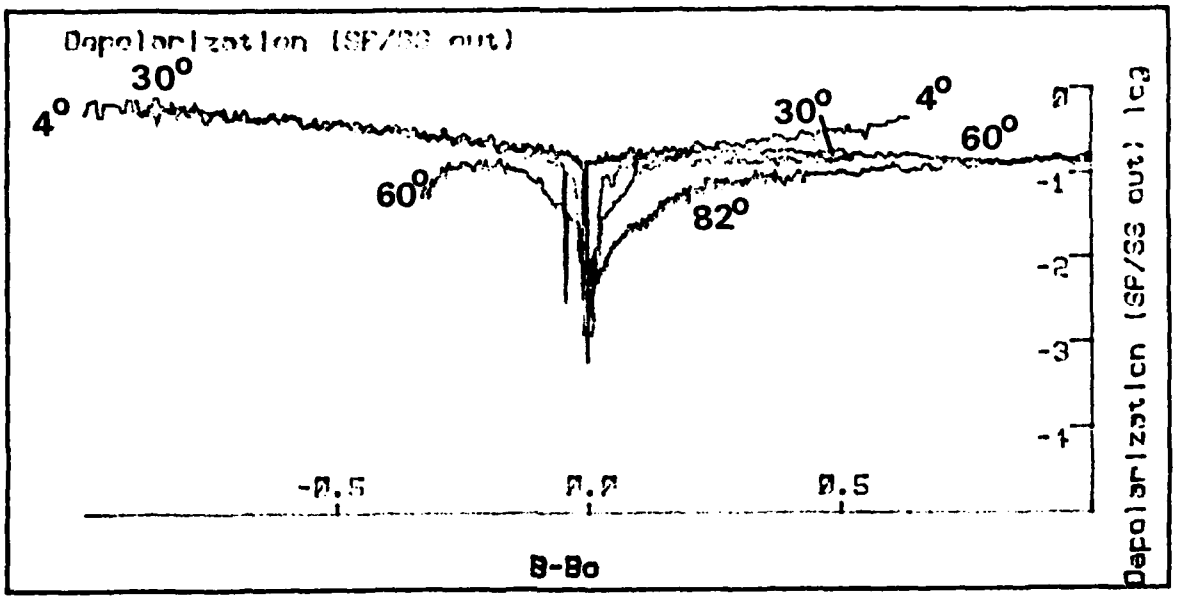


Figure 5.9 Depolarization versus direction cosines for the copper sample with 60 Angstroms of RMS roughness, and $\theta i$ = 4°, 30°, 60°, and 82°.

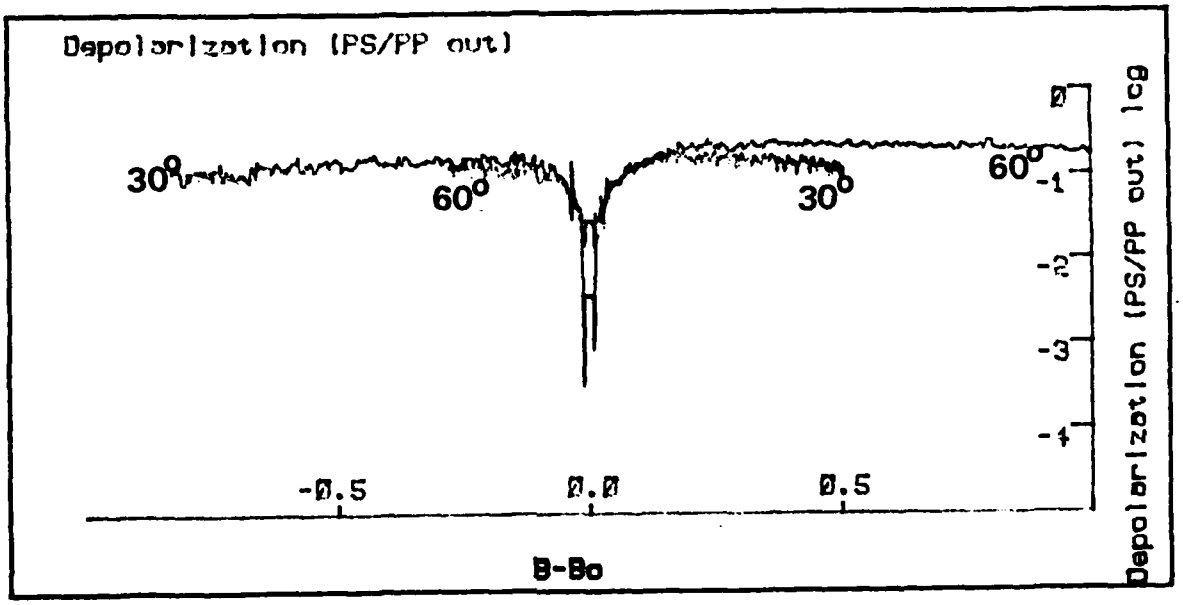


Figure 5.10 Depolarization versus direction cosines for the copper sample with RMS roughness of 60 Angstroms, and $\theta i$ = 30°, and 60°, and P input polarization.

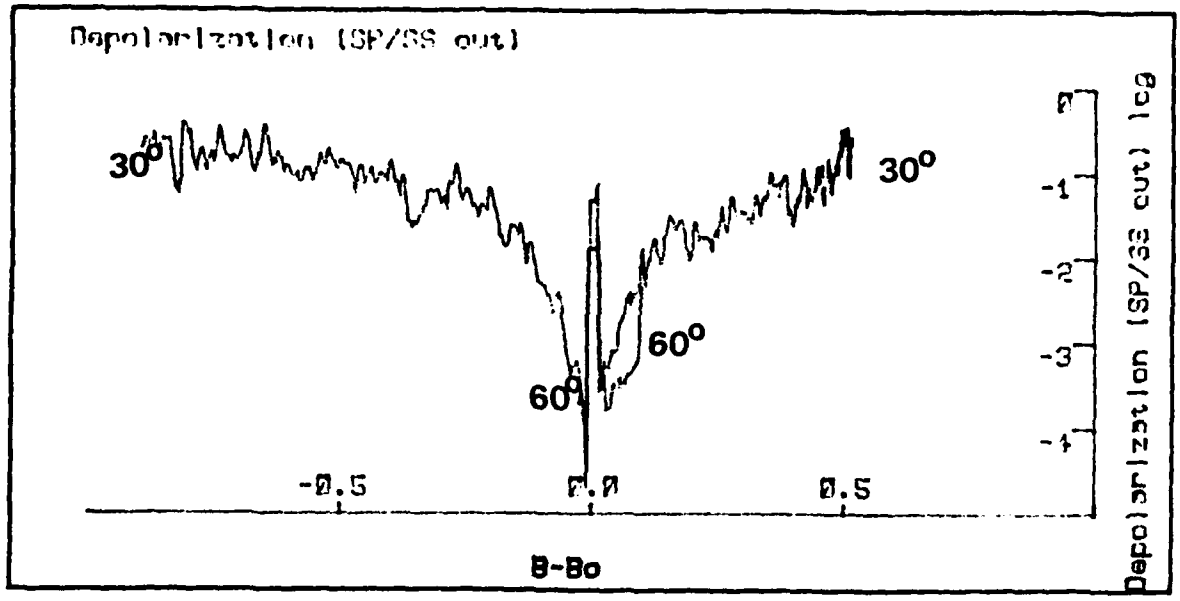


Figure 5.11 Depolarization versus direction cosines for the molybdenum sample with 45 Angstroms of RMS roughness, and θi = 30°, and θi = 60°.

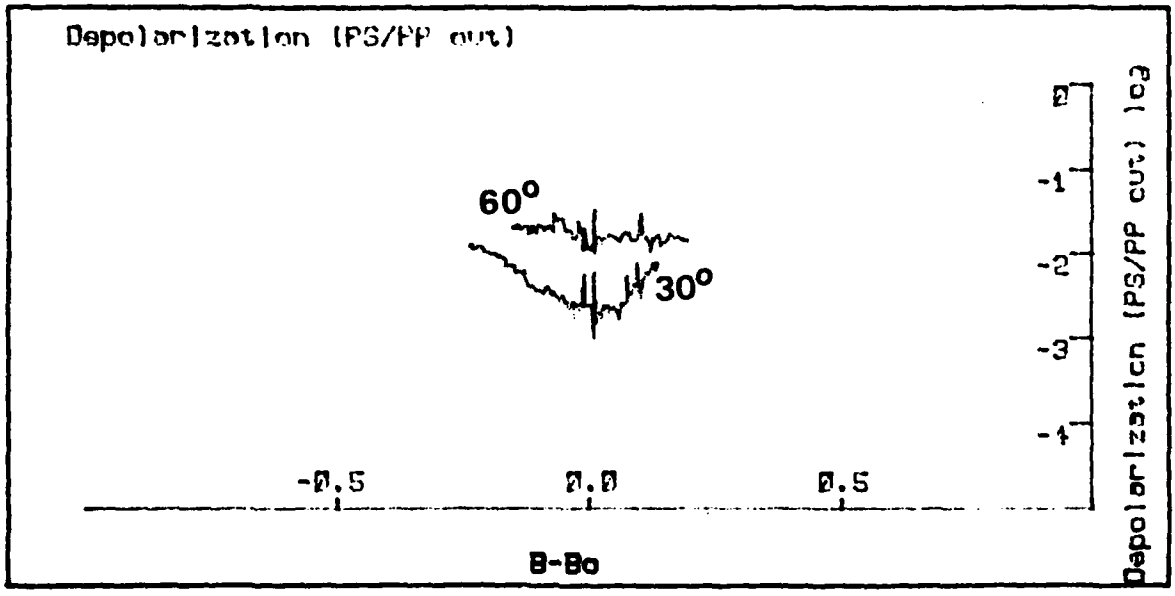


Figure 5.12 Depolarization versus direction cosines for the molybdenum sample with 45 Angstroms of RMS roughness, and θi = 30°, and 60°, and P input polarization.

# 6. DISCUSSION

In examining the results presented in Chapter 5 it is necessary to discuss how they compare with first order vector scatter theory and Bennett's results.(7) The results are evaluated to establish what trends, if any, can be found.

In examining the effect of using the exact form for the Q[SS] factor (equation 2.3 1) versus using the approximation (Q[SS]≈R[S]), the following observations can be made. First, a correction factor RMSQ/RMS can be used to correct the values of the calculated RMS roughness obtained using the approximation for the Q factor. Second, the Q factor changes both the shape and the magnitude of the PSD curve. The correction factor is different for different materials because the Q factor is a function of optical constants. In addition the calculated RMS roughness increases when the exact Q factor is used. This is because the correction factor is greater than 1. Note that the correction is greatest for samples with low values of reflectance, and that the correction factor is not necessarily the same for different surface morphologies. The possible difference in the correction factor is due to the integration of the PSD curve which includes the Q factor, over the range of spatial frequencies of observation. Because of this we have

implemented the Q factor into the calculations instead of using R[S].

Table 5.2 illustrates that the depolarization results measured at UNM are consistent with those reported by Bennett (7) at the Navel Weapons Center (NWC). Both the UNM and the NWC results for PP/SS are significantly lower than the theoretically predicted values. The results from UNM and NWC for depolarization (SP/SS) were comparable. This implies that the measurements made at UNM are consistent with other investigators, and they are lower than the theoretical predictions.

Figure 5.6 illustrates the results of examining depolarization as a function of RMS roughness for a number of copper samples. The RMS roughness for these samples ranged from 18 to 95 Angstroms. It can be seen that the depolarization characteristics for three of the samples are similar, while the sample with RMS roughness of 27 Angstroms is slightly lower for small scatter angles. The data for the copper samples with 18, 60, and 95 Angstroms of RMS roughness have PSD characteristics that are the same shape, and the amount of depolarization is approximately the same for them. For the sample with 27 Angstroms of RMS roughness the shape of the PSD characteristic is different. This indicates that the

distribution of microstructure for this sample is different from that of the other three, and that it is somewhat similar to the PSD characteristics of the molybdenum samples discussed below. This implies that depolarization is caused by the relative amount of high spatial frequency microroughness (i.e. short spatial wavelength) compared to the amount of low spatial frequency microroughness. This might explain the difference in the depolarization characteristics of this sample.

The optical scatter characteristics of two materials were examined; one material (copper) had a relatively higher amount of high spatial frequency microroughness than the other (molybdenum). Figures 5.4 and 5.5 illustrate this by showing typical PSD characteristics for each material. Note that the copper samples were actually Si wavers coated with different amounts of $CaF_2$ and then overcoated with 2000 Angstroms of evaporated copper. The molybdenum samples were polished from bulk molybdenum.

In order to be thorough, scatter was examined for both input polarizations. Note that for P input polarization, surface plasmons and other effects could influence the scatter. Data is included because of the interesting trends observed that warrant future

investigation. Figure 5.7 illustrates the depolarization of S polarized light by copper and molybdenum samples. Figure 5.8 illustrates depolarization for copper and molybdenum for P polarized light. The amount of depolarization for the molybdenum sample was much less than that for the copper sample. This result indicates that the type of surface microroughness has a large influence on the amount of depolarization. This further justifies the proposal above in connection with figure 5.6, that depolarization is caused by the relative amount of high spatial frequency microroughness compared to the amount of low spatial frequency microroughness. The molybdenum surface, on a relative bases has more low spatial frequency microroughness and less high spatial frequency microroughness compared to the copper samples examined.

Depolarization effects were examined as a function of incident angle for several samples. In the case of copper samples, depolarization is constant or it decreases slightly with increasing incident angle, for both input polarizations for angles far from the specular beam ($\theta s - \theta i > 30°$). For angles near the specular beam the amount of depolarization changed with increaseing incident angle. Figure 5.9 and 5.10, illustrate depolarization for a copper sample with various angles of incidence for both

input polarizations as shown. As angle of incidence increased, the amount of depolarization decreased symmetrically about the specular beam. This change in depolarization was not observed for the P input polarized light. The change in depolarization as a function of incident angle can not be attributed to shadowing of the surface morphology because, if it were due to shadowing, then the depolarization curves would not be symmetrical for angles near the specular beam ($\theta s - \theta i < 30°$).

In the case of molybdenum samples, depolarization illustrated a dependence on incident angle for P input polarization. Figure 5.12 illustrates depolarized scattered light with P polarized incident light. The depolarization increases significantly with changes in incident angle. However, no significant dependence was observed for S polarized light, which is illustrated in figure 5.11. These results imply that depolarization is very dependent on the spatial wavelength of the surface microroughness, Where as it is not extremely dependent upon the RMS roughness.

# 7. CONCLUSIONS

Depolarization from optical surfaces have been examined. The following conclusions can be made:

measurements of retroscatter ratios are comparable with results reported by Bennett (7); results are much lower than the theoretical predictions;

first order vector scatter theory does not predict depolarization in the plane of incidence; experimental data indicates that depolarization is present;

depolarization has little dependence on the RMS roughness of the surface for a specified surface morphology;

depolarization from surfaces with microstructure similar to that of copper is approximately constant with increasing angle of incidence, for both input polarizations;

depolarization from surfaces with relatively more large surface microstructure compared to copper (e.g. molybdenum), increase significantly with increasing angle of incidence for P input polarization, and is approximately constant for S input polarization.

Further investigations could be made in several directions. First, an investigation could be made to examine the results presented above using existing second order vector scatter theory which might explain the occurrence of depolarization in the plane of incidence. Second, a study could be made to extend the findings of this investigation to additional materials to see how the various surface microstructures effect the amount of depolarization. In this investigation the depolarization would be examined as a function of incidence angle to

determine what causes the depolarization to change and be symmetrical for angles near the specular beam. Third, an investigation examining depolarization as a function of light wavelength is warranted. This might provide an understanding of wavelength scaling and how light wavelength effects depolarization. Fourth, an investigation could be preformed to explain the discrepancy between the vector scatter theory and experimental results in the retroscatter ratios.

## REFERENCES


1. D.E. Barrick, "Scattering from Surfaces with Different Roughness Scales: Analysis and Interpretation," Battelle Memorial Institute. AD 662 751 (1967).

2. E.L. Church, and J.M. Zavada, "Residual Surface Roughness of Diamond-Turned Optics," Appl. Opt. **14**, 1788, (1975).

3. J.C. Stover, "Roughness Characterization of Smooth Machined Surfaces by Light Scattering," Appl. Opt. **14**, 1796, (1975).

4. G.R. Valenzuela, "Depolarization of EM Waves by Slightly Rough Surfaces," IEEE Transactions on Antenna and Propagation AP. **15**, 552, (1967).

5. S.O. Rice, "Reflection of Electromagnetic Waves from Slightly Rough Surfaces," Comm. Pure. Ap. Math. **4**, 351, (1951).

6. F. Jansen, "Investigation of the Surface Roughness of Evaporated Films by Optical Scattering," Ph D. Dissertation Case Western University, Cleveland Ohio, (1977).

7. J.M. Bennett, H.H. Hurt, J.P. Rhan, and J.M. Elson, "Relation Between Optical Scattering, Microstructure, and Topography of Thin Silver Films," Appl. Opt. **24**, 2701, (1985).

8. D.E. Barrick. Radar Cross Section Handbook Chap. 9. Plenum Press. Vol. 2 (1970).

9. E.L. Church H. A. Jenkinson and J.M. Zavada, "Relationship Between Surface Scattering and Microtopographic Features," Opt. Eng. **18**, 125, (1979).

10. J.M. Elson, and J.M. Bennett, "Vector Scatter Theory," Opt. Eng. **18**, 116, (1979).

11. J.E. Harvey, "Light Scattering Characteristics of Optical Surfaces," Phd Dissertation, University of Arizona, Tucson Ariz. (1976).

END

DTIC

9-86